THE JOURNAL OF PHYSICAL CHEMISTRY C

Article

pubs.acs.org/JPCC

Nonresonant Vibrational Energy Transfer on Metal Nanoparticle/Liquid Interface

Jiebo Li,[†,‡,⊥] Kaijun Yuan,[§,⊥] Hailong Chen,[‡] Andrea Miranda,[‡] Yuneng Shen,[§] Bo Jiang,[‡,§] Yajing Chen,[§] Yufan Zhang,[‡] Xunmin Guo,[‡] and Junrong Zheng*[,†,‡]

[†]College of Chemistry and Molecular Engineering, Beijing National Laboratory for Molecular Sciences, Peking University, Beijing 100871, China

[‡]Department of Chemistry, Rice University, Houston, Texas 77005, United States

[§]State Key Laboratory of Molecular Reaction Dynamics, Dalian Institute of Chemical Physics, Chinese Academy of Sciences, Dalian, Liaoning 116023, China

Supporting Information

ABSTRACT: Knowledge of vibrational energy transfer on a metal nanoparticle/liquid interface is essential for understanding the energy conversion process involved in many heterogeneous nanocatalyses. In this study, we investigate mode-specific vibrational energy transfer between CO molecules on different adsorbate sites on a 1 nm platinum metal nanoparticle/liquid interface by using ultrafast two-dimensional IR spectroscopy. The vibrational energy transport is found to be induced by vibration/vibration coupling with very little surface electron/vibration mediation. The energy transfer rate is determined to be about 1/140 ps^{-1} from the atop site CO to the bridge site CO, and the specific rate is around 1/400 ps^{-1} between the two nearest adsorbates. The energy transfer between different adsorbate sites can be described by the dephasing mechanism reasonably well. The mechanical coupling may contribute to the transfer, but analyses suggest that the role of dipole/dipole interaction is a more important factor for the energy transfer.

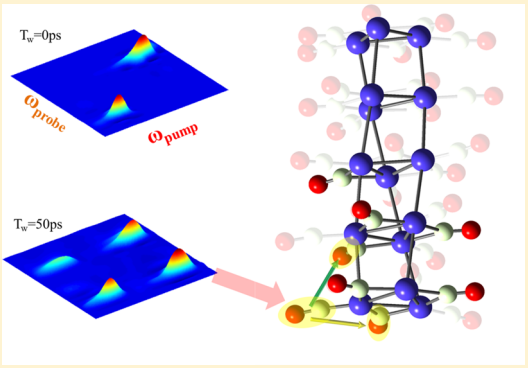

1. INTRODUCTION

The reaction selectivity and reaction rate are critical parameters to assess the performance of a heterogeneous catalyst.[1] In general, these two reaction properties are determined by the energy barrier of each possible reaction pathway, the local temperature, and the ability to cross the energy barriers.[1,2] The energy barriers are determined by static parameters, e.g. the molecular structures of the reactants and the detailed interactions among reactants, catalysts, and the environment. The local reaction temperature and the ability to cross the barriers are associated with dynamic processes, such as molecular energy transfers and dissipations among the reactants, catalyst, and solvent molecules.[3] Metal nanomaterials are typically the central component of the catalysts as the catalyzed reactions often occur on their surfaces.[4,5] On the surface of a metal nanoparticle, the molecular energy transfer and dissipation dynamics can be very unique, different from those in bulk liquids or solids because of the existence of a particle/liquid or particle/gas interface and the possible electron/vibration coupling between the surface free electrons of the particle and the vibrations of the surface molecules.[6] The importance and fascinating complexity of energy transfer dynamics on metal nanocatalyst surfaces have drawn many research efforts from both experiments and theory to investigate practical systems, model particle systems, and model clean surface systems using various approaches.[7−10] Knowledge on this topic has reached an unprecedented level.[3,11,12] However, many fundamental questions remain open: For example, is the electron/vibration coupling[13] between surface molecules and metal particle substrates ubiquitous? What is the relative importance between electron/vibration coupling and vibration/vibration coupling in mediating the vibrational energy dissipations of surface molecules? Which dominates the energy transfers among the vibrations of the surface molecules: the phonon compensation mechanism or the dephasing mechanism?[14−18]

Our previous studies of thiol molecules and CO molecules on the surfaces of a series of Au, Pt, and Pd nanoparticles demonstrated that both vibration/vibration and vibration/electron couplings are important to dissipate the vibrational energy of the molecules on the surfaces of these metal nanomaterials: (1) vibrations of a thiol molecule are 0.3 nm, or further, from the particle surface, and the vibration/vibration coupling dominates the dissipations;[19] (2) vibrations of

Received: April 13, 2016
Revised: June 2, 2016
Published: June 3, 2016

DOI: 10.1021/acs.jpcc.6b03777
J. Phys. Chem. C 2016, 120, 25173−25179

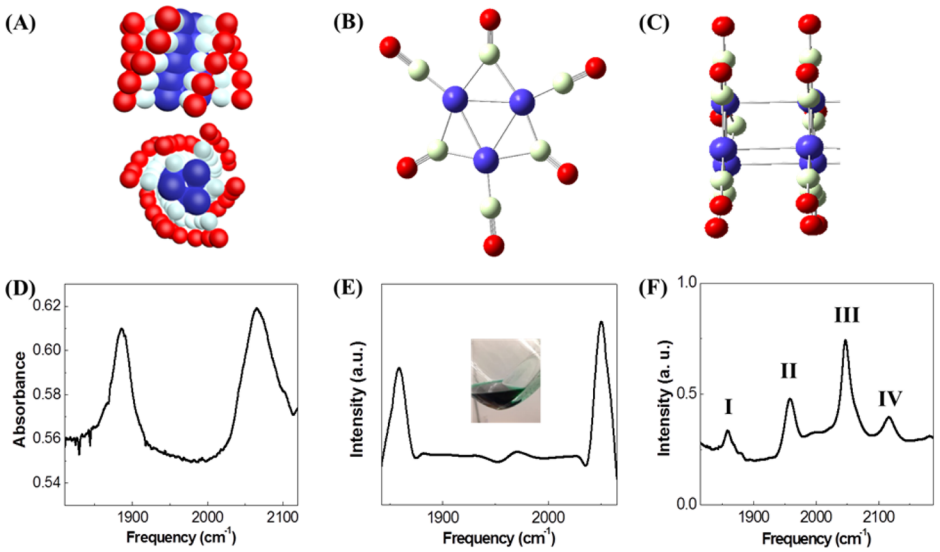

Figure 1. Structural and spectra information on CO coated 1 nm Pt sample. (A) Two views of the 1 nm Pt particle (purple, Pt; gray, C; red, O). (B) Structure of each triangular layer. (C) Structure between two layers. (D) FTIR spectrum of a 1 nm Pt particle powder sample in a vacuum. (E) FTIR spectrum of the 1 nm Pt particle in solution after the DMF solution background subtraction, showing the CO stretch frequencies. A picture of the solution sample is inserted. (F) FTIR spectrum of the 1 nm Pt particle without DMF background subtraction. Four peaks show up in the frequency range of the CO stretches. Peaks I and III are the mixtures of CO stretches and combination bands (or overtones) of DMF. Peaks II and IV are combination bands (or overtones) of DMF.

chemical bonds that directly interact with the surface electrons within the surface distance of about 0.2 nm, and the surface electron/hole pair transition dominates the relaxations.[20]

For vibrational relaxations that are dominated by vibration/vibration couplings on particle surfaces, after the initial intramolecular relaxations the energy eventually needs to transfer from one molecule to another to reach the final thermal equilibrium. In this work, we address a further question. If the particle system is in the liquid phase, how does this particle/liquid interfacial intermolecular energy transfer occur? Is it similar to those in crystalline solids, those in liquids, or something between? Our previous studies on model systems have suggested that, for noncoherent energy transfers which are defined as transfers with the energy donor/acceptor coupling strength smaller than the dephasing width of the donor/acceptor coherence,[21] resonant energy transfers in both liquids and solids can be described by the dephasing mechanism.[17] For nonresonant energy transfers which are defined as transfers with the central value of the energy distribution of the donor different from that of the acceptor, both the dephasing mechanism and phonon compensation mechanism play significant roles.[21] In crystalline solids, the phonon compensation mechanism can be dominant because the phonons with energy of the donor/acceptor gap can be abundant and the phase match conditions of phonons with the donor and acceptor have very few fluctuations.[15,21] However, the role of phonon compensation mechanism can be very minor in liquids.[15] In liquids, even if phonons, e.g. instantaneous normal modes,[21] with energy matching the donor/acceptor gap exist abundantly, the phonon compensation efficiency can still be very low. This is because during an energy transfer not only the total energy but also the total momentum needs to be conserved. The fast molecular motions, e.g. a donor and an acceptor switching their relative locations, result in a very similar modulation on both the donor and acceptor by a phonon which diminishes the phonon compensation efficiency.[15] An effective phonon compensation requires different modulations on the donor and the acceptor by the same phonon because the only possible way to convert two different things (donor/acceptor) to be the same is to make sure the actions on the two are different from each other.[15] The essential difference between the two energy transfer mechanisms is that, in the phonon compensation mechanism, the transfer is a one-step process where the donor transfers its energy to the acceptor of different energy and the donor/acceptor energy gap is compensated by emitting or absorbing phonons.[21] In the dephasing mechanism, the transfer is a "two-step process", in which the donor or acceptor first fluctuates to reach the same energy because of dephasing which is caused by molecular collisions and then energy resonantly transfers between them. In the dephasing mechanism, the energy fluctuation amplitude of the donor or acceptor does not have to match the phonon spectrum of the bath as molecular collisions that cause dephasing do not necessarily transfer their energy exclusively to change the energy of the donor/acceptor vibrational modes. On a particle/liquid interface, on one hand, the phonons of the particle can compensate the energy gap of the donor/acceptor bound on the particle surface. On the other hand, the solvent molecules in the liquid can cause the energy of the donor and acceptor to fluctuate and lead the dephasing energy transfer to occur. Therefore, it is not immediately clear which mechanism is more important for a nonresonant energy transfer on a particle/liquid interface.

In this work, we investigate nonresonant energy transfers on a liquid/particle interface by directly measuring the vibrational energy exchange dynamics between CO molecules on two different surface sites of an ~1 nm Pt particle in solution. We selected the 1 nm particle rather than the larger particles we previously studied[6] for the following two reasons: (1) The vibrational lifetimes of the CO molecules on the surface of 1 nm Pt particles are much longer than those of CO on the larger particles. On the larger Pt particles, the vibrational relaxations of CO are very short, lasting only a couple of picoseconds, because of the surface electron/vibration coupling. Due to the

DOI: 10.1021/acs.jpcc.6b03777
J. Phys. Chem. C 2016, 120, 25173−25179

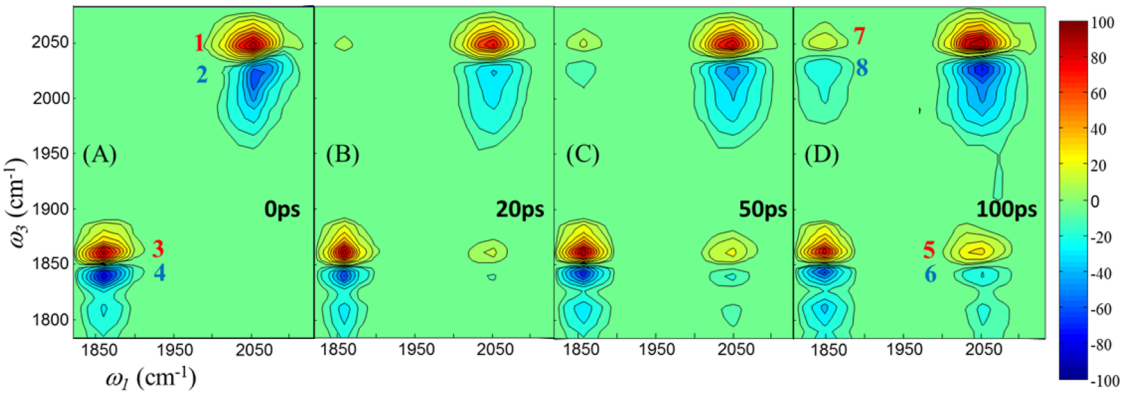

Figure 2. Time evolution of 2D IR spectra of the 1 nm Pt particle solution. The growth of the cross peak pairs (5, 6, 7, 8) indicate vibrational energy has exchanged between CO molecules on the atop and bridge sites.

very short lifetimes, the signals of slow direct vibrational energy exchanges among CO molecules on different surface sites are overwhelmed by heat signals. The much longer lifetimes of CO on 1 nm Pt particle allow the relatively slow energy exchange dynamics between CO molecules on different surface sites to be experimentally detected. (2) CO molecules on the 1 nm Pt surface have well-defined coordination sites on the surface. This is essential for our detailed analysis of the energy transfer process.

2. EXPERIMENTS

2.1. Optical Setup. The optical setup used for the ultrafast measurements has been described in our previous work.[22] Briefly, the ~80 MHz oscillator synchronizes two amplifiers (a picosecond amplifier and a femtosecond amplifier) with the same seeding pulse. By pumping an optical parametric amplifier (OPA), the picosecond amplifier produces ~0.8 ps mid-IR pulses with a bandwidth of 10−35 cm^{-1} in a tunable frequency range of 500−4000 cm^{-1} with energy ranging from 1 to 40 μJ/pulse at 1 kHz. This picosecond IR beam is the pumping beam in the pump−probe measurements. The probe pulse (~100 fs mid-IR pulses with a bandwidth of ~200 cm^{-1} in a tunable frequency range of 500−4000 cm^{-1} with energy ranging from 1 to 40 μJ/pulse at 1 kHz) is generated by the femtosecond amplifier. The signal detected is the probe beam intensity change, with the pump beam on and off. Two polarizers are positioned on the probe beam pathway (one of them is located immediately behind the sample) to selectively measure the parallel signal (I_{para}) or perpendicular (I_{perp}) polarized signal relative to the excitation beam. In particular, the pump focus beam spot is around ~300 μm and the pump pulse energy is around 5−10 μJ at 2047 cm^{-1}. The signal intensity presented here is the rotation-free data ($I_{Signal} = I_{para} + 2I_{perp}$). Because the sample is air-sensitive, the sample cell is placed in a vacuum chamber. The sample cell spacer is around 50 μm. Each nonlinear IR measurement is finished within a few hours.

2.2. Preparation of 1 nm Pt Nanoparticle. The sample preparation follows the reported method.[23] To summarize, 0.5 mL (0.1 M) aqueous solution of chloroplatinic acid ($H_2PtCl_6 \cdot 6H_2O$) dissolved in 10 mL of dimethylformamide (DMF) was reduced under CO atmosphere (1.5 atm) at room temperature for 28 h in a glass pressure vessel. Over the course of the reaction, the color of the solution changed gradually from yellow to blue-green. The final dark-green product in DMF was characterized by collecting the Fourier transform infrared (FTIR) spectrum (Figure 1A). The FTIR spectrum of the solid sample confirmed the formation of two CO species. However, the solid powder sample is not stable enough to perform ultrafast measurements. In this work, the measured dynamic data is from the sample in a solution of DMF.

3. RESULTS

3.1. Structure of the CO-Coated 1 nm Pt Particle. According to Longoni and Chini,[24] the structure of the CO-coated 1 nm Pt particle ($H_2[Pt_3(CO)_3(\mu_2\text{-}CO)_3]_5$) is illustrated in Figure 1A. The particle contains five layers of $Pt_3(CO)_3(\mu_2\text{-}CO)_3$ shown in Figure 1B. The distance between two layers is 3.03 Å (Figure 1C). On each layer, three Pt atoms form an equilateral triangle with the side length of 2.66 Å. One CO molecule (atop CO) binds on the top of each Pt atom with a Pt−C distance of 1.8 Å. Another CO molecule (bridge CO) sits between two Pt atoms with a Pt−C distance of 2.0 Å (the surface distance is ~1.55 Å). In a solid powder sample, the CO stretch frequency on the atop site is 2066 cm^{-1}, and that on the bridge site is 1887 cm^{-1} (Figure 1D). In a DMF solution, the frequencies are slightly shifted to 2047 and 1860 cm^{-1}, respectively (Figure 1E). These two CO stretch peaks overlap with dark modes (combination bands or overtones) of DMF (Figure 1F). Different from the FTIR measurements, the dark modes produce negligible signals (compared to those of CO) in two-dimensional (2D) IR measurements (Figure 2) and do not interfere with the CO signals. This is because the signal intensity of FTIR is proportional to the product of concentration times the transition dipole moment squared and that of 2D IR is proportional to the product of concentration times transition dipole moment to the fourth power.[25] The concentration of DMF is larger than that of Pt particles, but the transition dipole moments of the dark modes are much smaller than those of the CO stretches. Therefore, in the FTIR spectra, the dark mode peaks can have similar or even larger intensities than those of CO stretches, but their signals in 2D IR spectra are much smaller.

3.2. Vibrational Energy Exchange 2D IR Spectra. Figure 2 displays the time evolution of 2D IR spectra of the 1 nm Pt particle DMF solution. Using 2D IR spectroscopy to observe vibrational coupling and vibrational energy exchange has been thoroughly described for various systems, and further explanation can be found in refs 16 and 25−28. At time zero, only two diagonal peak pairs (peaks 1 and 2 and peaks 3 and 4) are observed in the 2D IR spectrum (Figure 2A). Peaks 1 and 2 are the 0−1 and 1−2 transition signals of the CO stretches on the atop site, respectively. Peaks 3 and 4 are the 0−1 and 1−2

DOI: 10.1021/acs.jpcc.6b03777
J. Phys. Chem. C 2016, 120, 25173−25179

transition signals of the CO stretches on the bridge site, respectively. The blue peaks 2 and 4 shift to lower frequencies along the *y*-axis from the respective red peaks because of vibrational anharmonicity, which causes a higher order vibrational transition to have a lower frequency than a lower order transition; e.g. the 1−2 transition frequency is smaller than that of the 0−1 transition of either CO stretch. In contrast to small metal carbonyl compounds,[29] the vibrational coupling cross peaks are very small in the 1 nm Pt particle system. They do not appear in Figure 2A because their relative intensities are less than 10% of the diagonal peak intensities. This 2D IR spectrum is distinctive in that the red peaks (0−1 transition) do not have a similar shape and intensity as their corresponding blue peaks (1−2 transition);[30] the blue peaks in Figure 2A are elongated along the *y*-axis and have smaller intensities, compared to the red peaks. The shapes of the blue peaks do not change with time (Figure 2B−D). These observations are similar to a Fermi resonance that occurs on the second excited state of an OD stretch that was described in detail previously.[31] Therefore, we tentatively attribute the unusual shapes of the blue peaks to Fermi resonances that occur on the second excited states of the CO stretches. It is also very likely that the feature is caused by ladder climbing in which CO is excited to higher excitation states. However, the higher order excitation will not affect our kinetic analysis because the vibrational lifetime used for the analysis is the measured value which is phenomenological.

With the increase in waiting time, vibrational energy begins to exchange between the CO molecules on the two surface sites and two cross peak pairs, 5 and 6 and 7 and 8, gradually grow (Figure 2B−D). The growth of peaks 5 and 6 shows that the vibrational energy has transferred from CO on the atop site to CO on the bridge site. Their excitation frequency (*x* coordinate) is 2050 cm^{-1}, which is the 0−1 transition frequency of CO on the atop site, indicating that the vibrational excitation originates from the excitation of the CO stretch on the atop site. Their detection frequencies (*y* coordinates) are 1860 cm^{-1} (peak 5) and 1836 cm^{-1} (the upper part of peak 6), which correspond to those of the 0−1 and 1−2 transition frequencies of CO on the bridge site, indicating that the detected vibrational excitation is that of CO molecules on the bridge site. Therefore, the growth rate of peaks 5 and 6 represents how fast the vibrational excitation transfers from the atop CO to the bridge CO. Similarly, the growth of peaks 7 and 8 indicates that the vibrational energy has transferred from the bridge CO to the atop CO. As discussed previously,[32] the vibrational energy exchange cross peaks are different from those of the chemical exchange cross peaks[30] in that the growth rate ratio of energy exchange cross peaks is determined by the detailed balance while that of chemical exchange cross peaks is 1:1. For the 1 nm Pt particle sample, the frequency difference between the two CO stretches is 187 cm^{-1}. At room temperature, the Boltzmann factor ($e^{-\Delta E/RT} = e^{-187/206}$) is 0.40, indicating that the energy transfer rate constant of the energy transfer process from the bridge CO to the atop CO must be only 40% of that from the atop CO to the bridge CO. Therefore, the upper cross peak pairs 7 and 8 should always be smaller than the lower peak pairs 5 and 6 at a given waiting time (Figure 2B−D). The location exchange between the two CO molecules is not observed within the time frame of our experiments (~200 ps). This is due to two reasons: (1) The binding energy of CO on Pt is much larger than 5 kcal/mol.[33,34] According to our previous studies on the correlation of binding energy and dissociation time,[35,36] such a binding energy suggests that the dissociation time of CO from the Pt surface must be slower than 1 ns. (2) All surface sites are occupied, meaning there is no room for location exchange unless CO desorption and readsorption occur very quickly, which is practically unlikely. The heat-induced cross peaks[22,25,37] are not observed in the system either. This is probably because the vibrational lifetimes are relatively long (40−50 ps) and the heat can dissipate rapidly into the solvent in which the concentration of the particles is very dilute (~300 μM). In addition, the heat response of the CO stretches that is determined by temperature dependence FTIR measurements is relatively small (see Supporting Information).

3.3. Vibrational Energy Exchange Kinetics. *3.3.1. Energy Exchange between One CO on One Site and All COs on the Other Site of the Same Particle.* Similar to our previous vibrational energy transfer experiments,[38−40] we construct a kinetic model to quantitatively analyze the vibrational energy exchange rate constants between CO molecules on the two surface sites. In our experiments, at most 1% of the CO molecules at each site are excited by the laser. Therefore, considering a single 1 nm Pt particle, the probability for only one CO molecule to be excited is much greater than that for multiple CO molecules to be excited. Detailed discussions are in the Supporting Information. Estimated from our previous experiments,[21,39] the nonresonant vibrational energy exchange between CO molecules on a surface site of one particle and CO molecules on another surface site of another particle must be slower than 1 ns in a dilute solution (300 μM). Therefore, the cross peaks 5−8 in Figure 2 are mainly from the vibrational energy exchange between CO molecules on different sites of the same particle. The excitations can also decay because of vibrational relaxations. In addition, the vibrational excitation of one CO molecule can also resonantly transfer to another CO molecule on the same surface site, which is much faster than the nonresonant transfer between CO molecules on different surface sites. However, such a resonant transfer does not cause the decrease of the vibrational excitation signal of the same CO species. The resonant energy transfer is not included. Therefore, in our energy transfer kinetic model, we use rotation-free data to analyze the nonresonant energy transfer rate constant from one CO molecule on one surface site to all CO molecules on the other surface sites. The kinetic model is depicted in Scheme 1.

Scheme 1. Excited Population Kinetic Model

$$\xleftarrow{k_{CO_{Bridge}}} \left[CO_{Bridge}\right] \underset{k_{Atop-Bridge}}{\overset{k_{Bridge-Atop}}{\rightleftharpoons}} \left[CO_{Atop}\right] \xrightarrow{k_{CO_{Atop}}}$$

Two differential equations can be derived from the kinetic model:

$$\frac{d[CO_{Bridge}]}{dt} = -(K_{CO_{Bridge}} + K_{Bridge-Atop})[CO_{Bridge}] + K_{Atop-Bridge}[CO_{Atop}] \quad (1)$$

and

$$\frac{d[CO_{Atop}]}{dt} = -(K_{Atop-Bridge} + K_{CO_{Atop}})[CO_{Atop}] + K_{Bridge-Atop}[CO_{Bridge}] \quad (2)$$

DOI: 10.1021/acs.jpcc.6b03777
J. Phys. Chem. C 2016, 120, 25173−25179

where $k_{Bridge-Atop}$ and $k_{Atop-Bridge}$ are the energy transfer rate constant from the bridge CO to the atop CO and the energy transfer rate constant from the atop CO to the bridge CO, respectively, and

$$\frac{k_{Bridge-Atop}}{k_{Atop-Bridge}} = e^{-\Delta E/RT} = e^{-187/206} = 0.40$$

$k_{CO_{Brdige}}$ and $k_{CO_{Atop}}$ are the vibrational relaxation rate constants of the bridge and atop CO. $[CO_{Bridge}]$ and $[CO_{Atop}]$ are the respective time dependent vibrational excitation populations of the bridge and atop CO modes. These excitation populations are obtained from the rotation-free intensities of the peaks in Figure 2. To determine $k_{Atop-Bridge}$, $[CO_{Atop}]$ is the intensity of peak 1 or 2 at each waiting time, and $[CO_{Bridge}]$ is the intensity of peak 5 or 6 at each waiting time. To determine $k_{Bridge-Atop}$, $[CO_{Atop}]$ is the intensity of peak 7 or 8 at each waiting time, and $[CO_{Bridge}]$ is the intensity of peak 3 or 4 at each waiting time. Calculations based on eqs 1 and 2 fit the experimental results well (Figure 3) and show that the energy transfer time

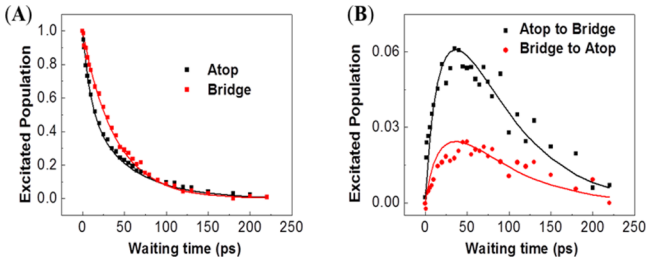

Figure 3. Rotation-free vibrational excitation populations and kinetic calculations. (A) Normalized intensity of peaks 1 (black) and 3 (red). (B) Normalized intensity of peaks 5 (black) and 7 (red). Dots are experimental data, and lines are calculations.

constant from the atop CO to the bridge CO is $\frac{1}{k_{Atop-Bridge}} = 140 \pm 40$ ps. The details of the fitting parameters are listed in the Supporting Information.

3.3.2. Vibrational Energy Exchange between the Nearest Atop–Bridge CO Pair. The energy transfer rate constant $k_{Atop-Bridge}$ determined above is from one donor on one site to all acceptors on the other site. This is because, on one particle, only one CO molecule can be excited by the laser and this excited CO molecule can transfer energy to all other CO molecules on the same particle (see discussion in the Supporting Information). Actually, on the 1 nm Pt sample, the excited CO on the atop site can dissipate the vibrational energy to a number of options. As shown in Figure 4, the first atop CO (the first layer, first site, 11) can (1) directly transfer energy to the nearby bridge CO (first layer, first site, 11) and (2) directly transfer energy to second layer COs and third layer COs on a bridge site. Equally, the excited bridge CO could meanwhile donate energy to a nearby atop CO. (See detailed expressions in the Supporting Information.) $[CO^{11}]_{Atop}$ represents CO on the first layer of the first atop site. Similarly, $k_{11Atop-11Bridge}$ and $k_{11Atop-21Bridge}$ represent the nonresonant energy transfer rate constant from this CO to CO on the first and second layer first bridge sites, respectively. If we assume that all atop COs have a same transition dipole and all the bridge COs also have another transition dipole, the vibrational energy transfer rate constant should be quantitatively related to the orientation factor κ and the distance r_{DA} between the donor

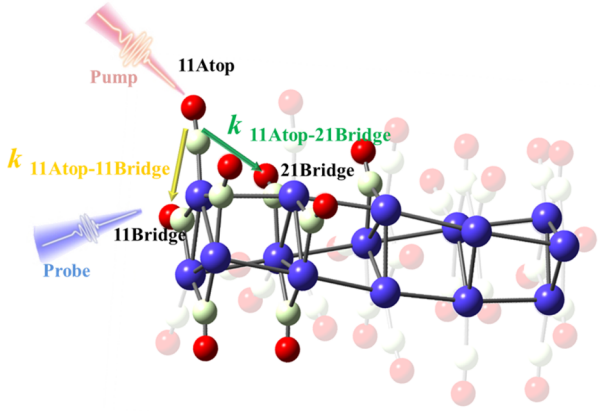

Figure 4. Demonstration of nonresonant energy transfer from the atop CO to the bridge CO (side view) on the 1 nm Pt sample. CO at 11Atop position is excited by an IR beam. The excitation energy then transfers from 11Atop to 11Bridge with rate constant $k_{11Atop-11Bridge}$ and to CO at 21Bridge with rate constant $k_{11Atop-21Bridge}$.

and acceptor based on the dipole–dipole coupling interaction,[21] as follows:

$$k \propto \beta^2 \propto \frac{\kappa^2}{r_{DA}^6} \quad (3)$$

With the calculation of κ and distance r_{DA} from structural information, we quantitatively obtain the relationship between each donor–acceptor pair energy transfer rate and $k_{11Atop-11Bridge}$.

$$K_{Atop-Bridge} = 3.3k_{11Atop-11Bridge}$$

Experimentally, the $k_{Atop-Bridge}$ is around $1/(140 \pm 40)$ ps^{-1}. Thus, the energy transfer rate from first layer, first atop CO to first layer, first bridge CO is around $1/(420 \pm 120)$ ps^{-1}.

4. DISCUSSION

The above quantitative results allow us to explore the mechanism for the nonresonant energy transfer on the particle/liquid interface: whether it is similar to the phonon compensation mechanism in some crystals or the dephasing mechanism in some liquids, or the combination of both.

On one hand, if the energy transfer process is dominated by the phonon compensation mechanism, the phonon modes around 187 cm^{-1} (the energy gap between the donor CO and the acceptor CO) should be present. However, due to the limit of our apparatus and the instability of the 1 nm Pt powder, we were not able to collect the terahertz (THz) spectrum of the 1 nm Pt powder. The THz spectrum of the DMF solution was collected, but there is no strong IR active phonon absorption in this frequency range (Figure S5). All the low frequency vibrations of the particle including Pt–Pt lattice vibration (around 170 cm^{-1}) are overwhelmed by the DMF background. In addition, phonons involved in the compensation for the energy transfer can be IR inactive, though an energy transfer in KSCN crystals previously studied is compensated by an IR active mode.[16] Therefore, the THz measurement does not contribute useful information for us to estimate the possibility of phonon compensation for the CO energy transfer.

On the other hand, for the dephasing mechanism, there are three factors determining the transfer rate: the energy mismatch

DOI: 10.1021/acs.jpcc.6b03777
J. Phys. Chem. C 2016, 120, 25173–25179

($\Delta\omega$ = 187 cm^{-1}), the dephasing time (τ), and the coupling strength (β). In this work, under the dipole/dipole approximation the coupling strength β was determined to be about 4.8 cm^{-1} between the first layer 11 atop CO and the 11 bridge CO with a given distance of 3.45 Å between the two molecules. The estimated dephasing time constant in solution is around 0.37 ± 0.06 ps by measuring the absorption line shape of the atop CO (in Supporting Information). Based on our previous work, if τ^{-1} (14.4 cm^{-1}) > β (4.8 cm^{-1}), the energy transfer rate constant can be described by eq 4.

$$k_{DA} = \frac{2}{1 + e^{-\Delta\omega/kT}}\beta^2\frac{1/\tau}{(\Delta\omega)^2 + 4\beta^2 + \tau^{-2}} \quad (4)$$

According to eq 4, k_{DA} is calculated to be 1/(395 ± 110) ps^{-1}. Compared with the experimentally determined value 1/(420 ± 120) ps^{-1}, the predicted value is consistent with the experiment value. This simple calculation suggests that the energy transfer process is likely through the dephasing mechanism: (1) First, molecular collisions between DMF solvent and CO induce the frequencies of COs on different sites fluctuating to reach the same value; (2) Then, the donor CO and acceptor CO exchange energy resonantly.

A couple of issues need to be clarified for the above discussion. First, dependent on the correlation between the dephasing events of the donor and acceptor, the dephasing line width can vary from 0 (perfect correlation) to the donor/acceptor line width sum (~29 cm^{-1}, no correlation). According to eq 4, this dephasing line width range can give a very large energy transfer rate variation. However, because the sample is in a room temperature liquid, it is expected that the donor and acceptor are not perfectly correlated. In addition, the donor/acceptor distance is 3.45 Å, which is close to the donor/acceptor distance of 4.0 Å in a previously studied system in which the dephasing line width is 50% of the line width sum.[16] It is reasonable to assume that in the current sample the dephasing line width should be similar or smaller. That is 7−14 cm^{-1}, resulting in k_{DA} values varying from about 1/400 to 1/800 ps^{-1}.

Second, in eq 4 the coupling strength β can be through any interaction,[14] e.g. dipole/dipole or mechanical coupling. In eq 3, only the dipole/dipole interaction is considered. The mechanical coupling is completely ignored. It is very likely that both mechanical coupling and dipole−dipole coupling are involved in the energy transfer. In the mechanical coupling mechanism, the transfer rate constant may not be exactly inversely proportional to r_{DA}^6. The power of the distance can be lower. To address this, we convert the experimental $k_{Atop-Bridge}$ into $k_{11Atop-11Bridge}$ based on the condition that the transfer rate constant is inversely proportional to r_{DA}^3, r_{DA}^4, or r_{DA}^5. The results are 1/714, 1/620, and 1/518 ps^{-1}, respectively. Based on eq 4, the pure dipole/dipole interaction gives 1/400−1/800 ps^{-1} as discussed above. If the mechanical coupling strength is the same as that of the dipole/dipole coupling strength, the total rate contributed by both couplings predicted by eq 4 is 1/100−1/200 ps^{-1}, which is much faster than the values derived from measurements. Therefore, the experimental results cannot exclude the contribution from the mechanical coupling, but at the same time they also suggest that the experimentally measured energy transfer rate is mainly contributed by the dipole/dipole interaction.

5. CONCLUDING REMARKS

By using ultrafast 2D IR spectroscopy, we measured the mode-specific vibrational energy transfer rate between COs on different adsorbate sites on a 1 nm Pt nanoparticle surface. The energy transfer between different adsorbate sites can be described by the dephasing mechanism reasonably well. The mechanical coupling may contribute to the transfer, but analyses suggest that the role of dipole/dipole interaction is a more important factor for the energy transfer.

■ ASSOCIATED CONTENT

Supporting Information

The Supporting Information is available free of charge on the ACS Publications website at DOI: 10.1021/acs.jpcc.6b03777.

Additional information that contains the kinetic model and calculations for energy transfer rates as noted in the text (PDF)

■ AUTHOR INFORMATION

Corresponding Author

*E-mail: zhengjunrong@gmail.com.

Author Contributions

⊥These authors contributed equally to this work.

Notes

The authors declare no competing financial interest.

■ ACKNOWLEDGMENTS

This work is supported by the Air Force Office of Scientific Research under AFOSR Award No. FA9550-11-1-0070, the Welch Foundation under Award No. C-1752, and the David and Lucile Packard Foundation. K.Y. is supported by the National Natural Science Foundation of China (No. 21373213), the Chinese Academy of Sciences, and the Ministry of Science and Technology.

■ REFERENCES

(1) Knözinger, H.; Kochloefl, K. Heterogeneous Catalysis and Solid Catalysts. *Ullmann's Encyclopedia of Industrial Chemistry*; Wiley: 2002.

(2) Froment, G. F.; Waugh, K. *Dynamics of Surfaces and Reaction Kinetics in Heterogeneous Catalysis*; Elsevier: 1997.

(3) Wodtke, A. M.; Matsiev, D.; Auerbach, D. J. Energy Transfer and Chemical Dynamics at Solid Surfaces: The Special Role of Charge Transfer. *Prog. Surf. Sci.* **2008**, *83*, 167−214.

(4) Tripa, C. E.; Yates, J. T. Surface-Aligned Reaction of Photogenerated Oxygen Atoms with Carbon Monoxide Targets. *Nature* **1999**, *398*, 591−593.

(5) Green, I. X.; Tang, W.; Neurock, M.; Yates, J. T. Spectroscopic Observation of Dual Catalytic Sites during Oxidation of CO on a Au/TiO2 Catalyst. *Science* **2011**, *333*, 736−739.

(6) Li, J.; Qian, H.; Chen, H.; Zhao, Z.; Yuan, K.; Chen, G.; Miranda, A.; Guo, X.; Chen, Y.; Zheng, N.; Wong, M. S.; Zheng, J. Two Distinctive Energy Migration Pathways of Monolayer Molecules on Metal Nanoparticle Surfaces. *Nat. Commun.* **2016**, *7*, 10749.

(7) Berkerle, J.; Casassa, M.; Cavanagh, R.; Heilweil, E.; Stephenson, J. Time Resolved Studies of Vibrational Relaxation Dynamics of CO (v= 1) on Metal Particle surfaces. *J. Chem. Phys.* **1989**, *90*, 4619−4620.

(8) Beckerle, J. D.; Casassa, M. P.; Cavanagh, R. R.; Heilweil, E. J.; Stephenson, J. C. Ultrafast infrared response of adsorbates on metal surfaces: Vibrational Lifetime of CO/Pt(111). *Phys. Rev. Lett.* **1990**, *64*, 2090−2093.

(9) Cavanagh, R. R.; Germer, T. A.; Heilweil, E. J.; Stephenson, J. C. Time-Resolved Measurements of Substrate to Adsorbate to Adsorbate Energy-Transfer. *Faraday Discuss.* **1993**, *96*, 235−243.

DOI: 10.1021/acs.jpcc.6b03777
J. Phys. Chem. C 2016, 120, 25173−25179

(10) Germer, T.; Stephenson, J.; Heilweil, E.; Cavanagh, R. Picosecond Measurement of Substrate-to-Adsorbate Energy Transfer: The Frustrated Translation of CO/Pt (111). *J. Chem. Phys.* **1993**, *98*, 9986.
(11) Krishna, V.; Tully, J. C. Vibrational Lifetimes of Molecular Adsorbates on Metal Surfaces. *J. Chem. Phys.* **2006**, *125*, 054706.
(12) Wodtke, A. M.; Tully, J. C.; Auerbach, D. J. Electronically Non-Adiabatic Interactions of Molecules at Metal Surfaces: Can We Trust The Born−Oppenheimer Approximation for Surface Chemistry? *Int. Rev. Phys. Chem.* **2004**, *23*, 513−539.
(13) Tully, J. C. Chemical Dynamics at Metal Surfaces. *Annu. Rev. Phys. Chem.* **2000**, *51*, 153−178.
(14) Chen, H. L.; Wen, X. W.; Guo, X. M.; Zheng, J. R. Intermolecular Vibrational Energy Transfers in Liquids and Solids. *Phys. Chem. Chem. Phys.* **2014**, *16*, 13995−14014.
(15) Chen, H. L.; Zhang, Q.; Guo, X. M.; Wen, X. W.; Li, J. B.; Zhuang, W.; Zheng, J. R. Nonresonant Energy Transfers Independent on The Phonon Densities in Polyatomic Liquids. *J. Phys. Chem. A* **2015**, *119*, 669−680.
(16) Chen, H. L.; Bian, H. T.; Li, J. B.; Wen, X. W.; Zhang, Q.; Zhuang, W.; Zheng, J. R. Vibrational Energy Transfer: An Angstrom Molecular Ruler in Studies of Ion Pairing and Clustering in Aqueous Solutions. *J. Phys. Chem. B* **2015**, *119*, 4333−4349.
(17) Chen, H.; Wen, X.; Li, J.; Zheng, J. Molecular Distances Determined with Resonant Vibrational Energy Transfers. *J. Phys. Chem. A* **2014**, *118*, 2463−2469.
(18) Kenkre, V. M.; Tokmakoff, A.; Fayer, M. D. Theory of Vibrational Relaxation of Polyatomic Molecules in Liquids. *J. Chem. Phys.* **1994**, *101*, 10618.
(19) Bian, H.; Li, J.; Chen, H.; Yuan, K.; Wen, X.; Li, Y.; Sun, Z.; Zheng, J. Molecular Conformations and Dynamics on Surfaces of Gold Nanoparticles Probed with Multiple-Mode Multiple-Dimensional Infrared Spectroscopy. *J. Phys. Chem. C* **2012**, *116*, 7913.
(20) Li, J.; Qian, H.; Chen, H.; Zhao, Z.; Yuan, K.; Chen, G.; Miranda, A.; Guo, X.; Chen, Y.; Zheng, N.; Wong, S. M.; Zheng, J. Two Distinctive Energy Migration Pathways of Monolayer Molecules on Metal Nanoparticle Surfaces. *Nat. Commun.* **2016**, *7*, 10749.
(21) Chen, H.; Wen, X.; Guo, X.; Zheng, J. Intermolecular Vibrational Energy Transfers in Liquids and Solids. *Phys. Chem. Chem. Phys.* **2014**, *16*, 13995−14014.
(22) Chen, H.; Bian, H.; Li, J.; Wen, X.; Zheng, J. Relative Intermolecular Orientation Probed via Molecular Heat Transport. *J. Phys. Chem. A* **2013**, *117*, 6052−6065.
(23) Chen, G.; Yang, H.; Wu, B.; Zheng, Y.; Zheng, N. Supported Monodisperse Pt Nanoparticles from [Pt3 (CO) 3 (μ2-CO) 3] 52-Clusters for Investigating Support-Pt Interface Effect in Catalysis. *Dalton Trans.* **2013**, *42*, 12699−12705.
(24) Longoni, G.; Chini, P. Synthesis and Chemical Characterization of Platinum Carbonyl Dianions [Pt3 (CO) 6] n2-(n = . apprx. 10, 6, 5, 4, 3, 2, 1). A new Series of Inorganic Oligomers. *J. Am. Chem. Soc.* **1976**, *98*, 7225−7231.
(25) Chen, H.; Bian, H.; Li, J.; Wen, X.; Zheng, J. Ultrafast Multiple-Mode Multiple-Dimensional Vibrational Spectroscopy. *Int. Rev. Phys. Chem.* **2012**, *31*, 469−565.
(26) Asbury, J. B.; Steinel, T.; Fayer, M. D. Using Ultrafast Infrared Multidimensional Correlation Spectroscopy to Aid in Vibrational Spectral Peak Assignments. *Chem. Phys. Lett.* **2003**, *381*, 139−146.
(27) Khalil, M.; Demirdoven, N.; Tokmakoff, A. Coherent 2D IR Spectroscopy: Molecular Structure and Dynamics in Solution. *J. Phys. Chem. A* **2003**, *107*, 5258−5279.
(28) Cervetto, V.; Helbing, J.; Bredenbeck, J.; Hamm, P. Double-Resonance versus Pulsed Fourier Transform Two-Dimensional Infrared Spectroscopy: An Experimental and Theoretical Comparison. *J. Chem. Phys.* **2004**, *121*, 5935−5942.
(29) Khalil, M.; Demirdoven, N.; Tokmakoff, A. Vibrational Coherence Transfer Characterized with Fourier-Transform 2D IR Spectroscopy. *J. Chem. Phys.* **2004**, *121*, 362−373.
(30) Zheng, J.; Kwak, K.; Asbury, J. B.; Chen, X.; Piletic, I.; Fayer, M. D. Ultrafast Dynamics of Solute-Solvent Complexation Observed at Thermal Equilibrium in Real Time. *Science* **2005**, *309*, 1338−1343.
(31) Zheng, J.; Kwak, K.; Steinel, T.; Asbury, J. B.; Chen, X.; Xie, J.; Fayer, M. D. Accidental Vibrational Degeneracy in Vibrational Excited States Observed with Ultrafast Two-Dimentional IR Vibrational Echo Spectroscopy. *J. Chem. Phys.* **2005**, *123*, 164301.
(32) Bian, H.; Wen, X.; Li, J.; Chen, H.; Han, S.; Sun, X.; Song, J.; Zhuang, W.; Zheng, J. Ion Clustering in Aqueous Solutions Probed with Vibrational Energy Transfer. *Proc. Natl. Acad. Sci. U. S. A.* **2011**, *108*, 4737−4742.
(33) Yamagishi, S.; Fujimoto, T.; Inada, Y.; Orita, H. Studies of CO Adsorption on Pt(100), Pt(410), and Pt(110) Surfaces Using Density Functional Theory. *J. Phys. Chem. B* **2005**, *109*, 8899−8908.
(34) Orita, H.; Inada, Y. DFT Investigation of CO Adsorption on Pt (211) and Pt (311) Surfaces from Low to High Coverage. *J. Phys. Chem. B* **2005**, *109*, 22469−22475.
(35) Zheng, J.; Kwak, K.; Chen, X.; Asbury, J. B.; Fayer, M. D. Formation and Dissociation of Intra-intermolecular Hydrogen Bonded Solute-Solvent Complexes: Chemical Exchange 2D IR Vibrational Echo Spectroscopy. *J. Am. Chem. Soc.* **2006**, *128*, 2977−2987.
(36) Zheng, J.; Fayer, M. D. Solute-Solvent Complex Kinetics and Thermodynamics Probed by 2D-IR Vibrational Echo Chemical Exchange Spectroscopy. *J. Phys. Chem. B* **2008**, *112*, 10221.
(37) Bian, H. T.; Zhao, W.; Zheng, J. R. Intermolecular Vibrational Energy Exchange Directly Probed with Ultrafast Two Dimensional Infrared Spectroscopy. *J. Chem. Phys.* **2009**, *131*, 124501.
(38) Bian, H.; Li, J.; Wen, X.; Zheng, J. R. Mode-Specific Intermolecular Vibrational Energy Transfer: 1. Phenyl Selenocyanate and Deuterated Chloroform Mixture. *J. Chem. Phys.* **2010**, *132*, 184505.
(39) Bian, H.; Chen, H.; Li, J.; Wen, X.; Zheng, J. Nonresonant and Resonant Mode-Specific Intermolecular Vibrational Energy Transfers in Electrolyte Aqueous Solutions. *J. Phys. Chem. A* **2011**, *115*, 11657−11664.
(40) Bian, H. T.; Wen, X. W.; Li, J. B.; Zheng, J. R. Mode-Specific Intermolecular Vibrational Energy Transfer. II. Deuterated Water and Potassium Selenocyanate Mixture. *J. Chem. Phys.* **2010**, *133*, 034505.

DOI: 10.1021/acs.jpcc.6b03777
J. Phys. Chem. C 2016, 120, 25173−25179